J Seismol (2012) 16:829–838
DOI 10.1007/s10950-012-9301-z

ORIGINAL ARTICLE

Effects of rotation motions on strong-motion data

H. C. Chiu · F. J. Wu · C. J. Lin · H. C. Huang · C. C. Liu

Received: 23 August 2011 / Accepted: 13 March 2012 / Published online: 1 April 2012

Abstract Rotation motion and its effects on strong-motion data, in most cases, are much smaller than that of translational motion and have been ignored in most analyses of strong-motion data. However, recent observations from near-fault and/or extreme large ground motions suggest that these effects might be underestimated and quantitative analyses seem to be necessary for improving our understating of these effects. Rotation motion-related effects include centrifugal acceleration, the effects of gravity and effects of the rotation frame. Detailed analyses of these effects based on the observed data are unavailable in the literature. In this study, we develop a numerical algorithm for estimating the effects of rotational motion on the strong-motion data using a set of six-component ground motions and apply it to a set of rotation rate-strong motion velocity data. The data were recorded during a magnitude 6.9 earthquake. The peak value of the derived acceleration and rotation rate of this dataset are about 186 cm/s/s and 0.0026 rad/s. Numerical analyses of data gives time histories of these rotational motion-related effects. Our results show that all the rotation angles are less than 0.01°. The maximum centrifugal acceleration, effect from gravity and effect of the rotation frame are about 0.03 and 0.14 cm/s/s, respectively. Both these two effects are much smaller than the peak acceleration 186 cm/s/s. This result might have been expected because our data are not near-field and wave motions are expected to be nearly plane waves. However, it is worth noticing that the centrifugal acceleration is underestimated and a small rotational effect can cause large waveform difference in acceleration data. The waveform difference before and after the correction for rotational motion can reach 16 cm/s/s (about 10 %).

Keywords Translational motions · Rotational motions · Strong motion · Ground tilt · Centrifugal acceleration

H. C. Chiu (✉) · F. J. Wu · C. J. Lin · C. C. Liu
Institute of Earth Sciences, Academia Sinica,
P.O. Box 1-55, Nankang,
Taipei 115, Taiwan
e-mail: chiu@earth.sinica.edu.tw

H. C. Huang
Institute of Seismology, National Chung-Chen University,
Minhsiung, Taiwan

1 Introduction

Accelerographs were designed mainly for measuring three-component translational ground motions. Accelerometers can also detect rotational motion and its induced effects. These effects including centrifugal acceleration, gravity (tilt) effects, and effects of rotation frame (coordinate system) have been ignored in most analyses of strong-motion data because these effects are much smaller than that of the corresponding translational motions. However, more and more observations from near-fault and/or extreme large ground motion records indicate that these effects might be underestimated. Furthermore, the relationships between peak values of a vertical rotational rate and horizontal translational motion show that the rotational motion might increase with an increase in ground motion (Lee et al. 2009; Takeo 2009). Therefore, the behavior of an inertial sensor due to complex loading (both of translational and rotational motions) and the effects of rotational motion on strong-motion data have attracted more attention (e.g., Pillet and Virieux 2007; Graizer and Kalkan 2008).

The effect of rotational motion on strong-motion waveforms have been less studied. The first effect is the centrifugal acceleration which pulls the rotation object (the mass of the accelerometer) away from the rotation center. This induced centrifugal acceleration was well estimated in a robot-arm-movement experiment, where the rotation arm (robot arm) is 0.96 m, and the rotation rate is 0.251 rad/s results in a centrifugal acceleration of 6 cm/s/s (Lin et al. 2010). Previously, the induced centrifugal acceleration in strong-motion record was believed to be very small and could be discounted (Graizer 2009). According to Graizer's estimates, the length of the spring of a seismometer usually does not exceed 20 cm and the highest angular velocity observed during earthquakes does not exceed 0.2 rad/s, with an induced centrifugal acceleration less than 0.8 cm/s/s. The second effect is the gravity-related effect. If the ground has a tilt due to a permanent deformation or rotation motion, the contribution to the two horizontal components from gravity will change and reduce its effect on the vertical component. This effect has been most often discussed as related to the recovery of permanent displacement from strong-motion acceleration data (Boore 2001; Boroschek and Legrand 2006; Graizer 2005). Although the cause of baseline drift of this type in a strong-motion record is not well understood, it is widely believed that the ground tilt contributes the most to the baseline drift which occurs in the central body of a record. The last effect is due to the changing frame with time. If the ground has a rotation motion, the accelerograph attached to the ground will be on a rotation frame where the orientation changes over time; therefore, any component of the recorded ground motions is no longer moving in the same direction. This effect was discussed in the robot-arm-movement experiment (Lin et al. 2010) but no similar discussion of this effect on strong-motion data can be found.

In order to obtain more information about these three types of effects, we estimate these effects within a time domain. We numerically solve the attitude equation and equation of motion in the rotation frame using a set of six-component ground motion data. The results provide three-component time histories of Euler's angles, centrifugal accelerations, and gravity effects. With this set of information, we can further calculate the translational motions in the reference frame and estimate the effects of a rotation frame on the translational motions.

2 Data and data processing

The data selected in this study were recorded at seismographic station HWLB during the December 19, 2009 earthquake in Taiwan. This earthquake, registered 6.9 in local magnitude with a focal depth of 44 km, is the largest event occurring during our experimental deployment from May 2008 to November 2011. The epicenter was located in the south of HWLB and the epicenter distance was about 21 km.

The HWLB located at a branch office of the Central Weather Bureau in Hualien, Taiwan. The deployment at HWLB includes one R1 (Nigbor et al. 2009) rotation sensor and one VSE-355 G3 (Clinton and Heaton 2003; Hutt et al. 2008) strong-motion velocity seismometer with a six-channel Quanterra 24-bit Q330 data logger. This instrumentation was deployed next to a strong-motion accelerograph (station code of HWA019) which is one station of an island-wide strong-motion network of the Taiwan Strong Motion Installation Program. All these instruments lay upon a deep silty or clayey gravel deposits. The exact depth of the bedrock is not known. However, according to a nearby 200-m drill (which did not hit the bedrock), the thickness of deposit under the HWLB is expected to be more than 200 m. A borehole velocity logging for the HWA019 shows that the V_{30} at this site is 503.5 m/s.

Our analyses require both the three-component rotation rate and three-component acceleration waveforms with a common timing system as inputs. It is necessary to convert these strong-motion velocity waveforms from a VSE-355 G3 velocity to acceleration. Because the VSE-355 G3 seismometers show a flat frequency response from 0.02 to 100 Hz (Hutt et al. 2008), we did not apply any instrument correction for the velocity waveform here. To covert the velocity waveforms to acceleration, we used a numerical differentiation. The sampling interval (Δt) of the velocity waveform is 0.01 s. To retain a zero-time shift when taking a numerical differentiation, we used a cubic-spline interpolation to obtain the velocities at $t-0.5\Delta t$ and $t+0.5\Delta t$ which can be used further in the two-point numerical differentiation for obtaining the acceleration at time t.

To check this conversion, we compared these derived acceleration waveforms with an independent observation at station HWA019. The comparisons of waveforms and Fourier amplitude spectra between the derived and observed acceleration time histories are shown in Fig. 1. For all the figures shown here, the three-component waveforms and spectra are normalized by their maximum and are arranged to be, the north–south, east–west, and vertical components from top to the bottom. For purposes of comparison as shown in Fig. 1, waveforms and Fourier amplitude spectra of both HWLB and HWA019 are further normalized to the same scale. As shown in Fig. 1, there is no significant difference between waveforms and spectra. The correlation coefficients between these two types of waveforms are 0.9990, 0.9986, and 0.9711 in the north–south, east–west, and vertical components, respectively.

The instrument response of the R1 sensor (30 s–50 Hz version) is corrected by poles and zeros provided by the manufacturer (eentec). Since the major signal for rotational rate is in the range from 0.5 to 15 Hz, where the R1 sensor has a flat response (Nigbor et al. 2009), the changes in waveform after the instrument correction is small and the correlation coefficients between the waveforms before and after correction are 0.9890, 0.9869, and 0.9890 for the north–south, east–west, and vertical components, respectively. The time shift of the waveform due to the non-zero phase of the R1 transfer function is also estimated to be less than one sampling interval (0.01 s).

Because the rotational and the translational sensors have a different frequency response, we apply a same band-pass filter (from 0.1 to 20 Hz) to both types of waveforms to estimate the rotational effects. The final waveforms after conversion, instrument correction,

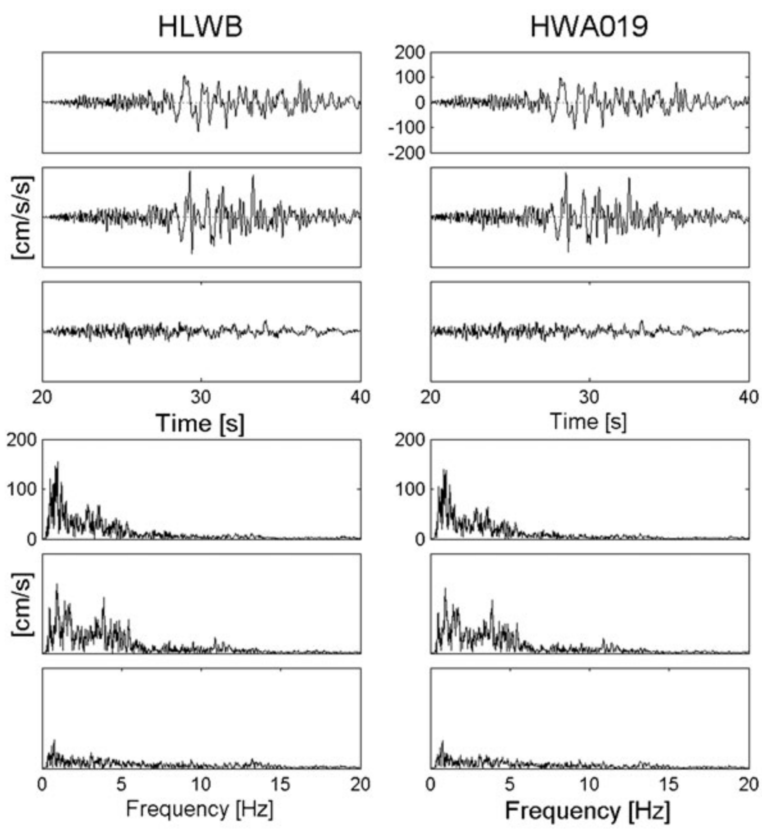

Fig. 1 Comparisons of waveforms (*upper three rows*) and Fourier amplitude spectra (*lower three rows*) between the derived accelerations (*left*) and a strong-motion acceleration record (*right*). The derived acceleration is obtained by numerical differentiation of the broadband velocity data recorded at HWLB while the HWA019 is from an independent observation collocated with HWLB

baseline correction, and band-passed filtering are shown in Fig. 2. The maximum rotation rate of two horizontal components are about 2×10^{-3} rad/s while the vertical component is about 5×10^{-4} rad/s. The peak ground acceleration is about 186 cm/s/s in the horizontal component and about 52 cm/s/s in the vertical component.

3 Method

The method used in this analysis is similar to the approach used in the robot-arm-experiment (Lin et al. 2010) except the rotational data have been corrected for instrument response and both the rotation rate and the ground motion data have been corrected for baseline error (Chiu 1997). The baseline correction is necessary for this study. Without a baseline correction, the accumulated low-frequency error might result in an unstable solution. This is particularly important for the rotation data which has much lower signal-to-noise ratio than that of the translational motion.

Before a more detailed discussion of our method, we need to define three types of frames. A schematic illustration of the relationship among the rotational frame, the translational frame, and the reference frame is given in Fig. 3. We select the coordinate system before the seismic loading as a reference frame "Ref". If the sensor has a pure translational motion from "Ref" to "Trans", then a three-component motion can describe this type of motion. When a sensor moves from "Ref" to "Rot", except for the three-component translational motion, an additional three-component rotational motion is required to fully describe the sensor moving.

If the ground movement involves rotational motion, the explicit form of the equation of motion can be given in the rotation frame as

$$\ddot{U}^R(t) = A^R(t) - \dot{\Theta}^R(t) \times \dot{U}^R(t) - G^R(t) \tag{1}$$

In this equation and the following discussion, the symbols in capital letters represent a vector or a matrix and the superscript "R" of a parameter denotes that the parameter is measured in the rotation frame. In Eq. (1), acceleration $\ddot{U}^R$ and velocity $\dot{U}^R$ of the ground are two unknowns to be solved while A^R and $\dot{\Theta}^R$ are the observed acceleration and rotation rate in the rotation frame. The second and the third terms on the right of Eq. (1) are effects due to the presence of the rotation motions; the second term is the induced centrifugal acceleration which is equivalent to the cross product of the rotation rate and velocity vector. The third term G^R is the effective gravity on three components. The vector G^R can be obtained if the Euler angels are given and more detailed discussion about G^R is presented later.

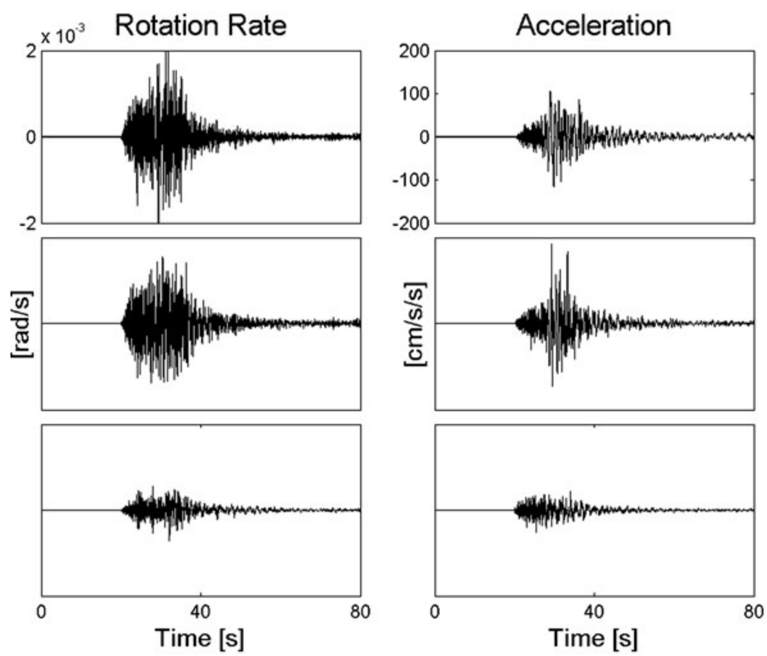

Fig. 2 Three-component rotation rate (*left*) and ground acceleration (*right*) used in this study. From *top* to the *bottom* are east, north, and up directions. The acceleration is derived from the broadband velocity seismogram by numerical differentiation

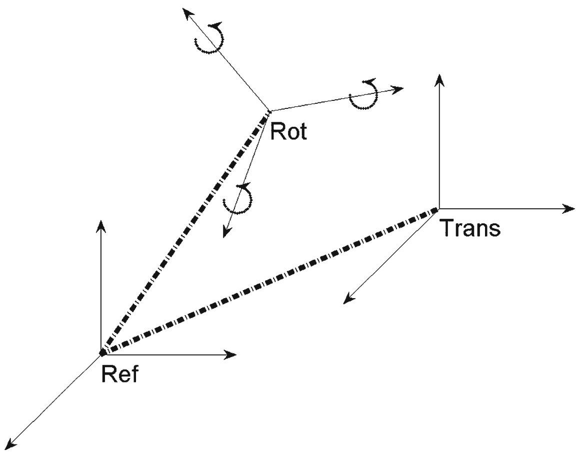

Fig. 3 Schematic demonstration of the relationship between a rotational frame ("*Rot*") and a translational frame ("*Trans*") related to the reference frame ("*Ref*")

Equation (1) can be rewritten as an ordinary differential equation of $\dot{U}^R$

$$\frac{d\dot{U}^R(t)}{dt} = A^R(t) - \dot{\Theta}^R(t) \times \dot{U}^R(t) - G^R(t) \tag{2}$$

To solve this equation, first we need to calculate G^R and the calculation of G^R from G requires a set of transformation matrix which is defined by a set of Euler's angles $\Psi = (\alpha \quad \beta \quad \gamma)$. Euler's angles cannot be obtained directly from the rotation rate function because the rotation rate functions are measured in the rotation frame. To calculate Euler's angles as time functions, we need to solve the attitude equation (Lin et al. 2010).

$$\begin{pmatrix} \dot{\alpha} \\ \dot{\beta} \\ \dot{\gamma} \end{pmatrix} = \begin{pmatrix} 1 & s_1 \tan\beta & c_1 \tan\beta \\ 0 & c_1 & -s_1 \\ 0 & s_1 \sec\beta & c_1 \sec\beta \end{pmatrix} \begin{pmatrix} \dot{\theta}_x \\ \dot{\theta}_y \\ \dot{\theta}_z \end{pmatrix} \tag{3}$$

This equation is another ordinary differential equation of α, β, and γ which can be solved numerically. After solving Eq. (3), we obtain the time functions of α(t), β(t), and γ(t) which can be further applied to calculate G^R and to transform the ground motions from rotation frame to the reference frame.

The gravity effect G^R in Eq. (2) is the change of gravity before and after the present of rotation motions, therefore

$$G^R = G - T_3T_2T_1G = \begin{pmatrix} 0 \\ 0 \\ g \end{pmatrix} - \begin{pmatrix} c_3 & -s_3 & 0 \\ s_3 & c_3 & 0 \\ 0 & 0 & 1 \end{pmatrix} \begin{pmatrix} c_2 & 0 & s_2 \\ 0 & 1 & 0 \\ -s_2 & 0 & c_2 \end{pmatrix} \begin{pmatrix} 1 & 0 & 0 \\ 0 & c_1 & -s_1 \\ 0 & s_1 & c_1 \end{pmatrix} \begin{pmatrix} 0 \\ 0 \\ g \end{pmatrix} = \begin{pmatrix} -gs_2 \\ gc_2s_1 \\ -g(1-c_1c_2) \end{pmatrix} \tag{4}$$

Where $s_1 \equiv \sin\alpha$, $c_1 = \cos\alpha$, $s_2 = \sin\beta$, etc.

Substituting (4) and two known variables A^R and $\dot{\Theta}^R$ to (2) and solving differential equation gives $\dot{U}^R$. The pure translational motion in the rotation frame $\dot{U}^R$ can be transformed to a reference frame using the same transformation matrix as that in Eq. (4) and results in the translational velocity in the reference frame $\dot{U}$. The translational acceleration in the reference frame can be derived from $\dot{U}$ by a numerical differentiation or by Eq. (1).

4 Results and discussion

Solving Eq. (3) gives the time functions of Euler's angels $\alpha(t)$, $\beta(t)$, and $\gamma(t)$. Plots of these time functions are given in Fig. 4. These time histories differ from the integration of the rotation rate functions because the latter in the rotational frame constantly changes its orientation during the seismic loading. The similarity between time histories of Euler's angles and the acceleration waveforms implies that rotational motion always exists and the amount of rotational motions is in proportion to the translational motions. The maximum Euler's angle, as shown in Fig. 4., is about 0.01° which indicates that the rotational motions are moving within a very small range.

Before solving Eq. (2), we examine the centrifugal acceleration and the gravity effects. As shown in Fig. 5, the centrifugal acceleration of the vertical component has a larger value and appears to have an asymmetric time history. The peak centrifugal acceleration is about 0.03 cm/s/s which is much larger than the conventional estimates (e.g., Graizer 2009). Following Graizer's approach and keeping the same length of the spring at 20 cm, the induced centrifugal acceleration is less than 0.000135 cm/s/s as the highest angular velocity in this case is 0.0026 rad/s. This estimation is much smaller

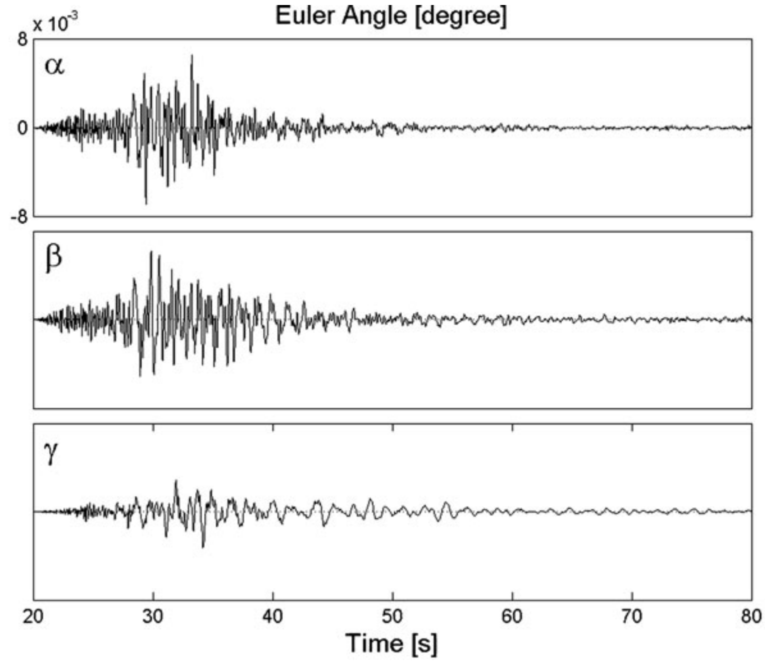

Fig. 4 Three-component Euler's angles (*degrees*). The maximum is about 0.01°

than our result, 0.03 cm/s/s. In fact, the VSE-355 G3 belongs to the mass-on-spring type sensor which has much shorter length of the spring and will cause even smaller centrifugal acceleration. The discrepancy implies that the center of rotation motion is not at the fixed point of the spring in the seismometer.

The estimated effects of gravity using Eq. (4) are shown in Fig. 6. The time histories of two horizontal components are similar to the ground-motion waveform and both have a similar peak value of about 0.15 cm/s/s. It is worth noticing that the effects of gravity in the vertical component are much smaller than those of the

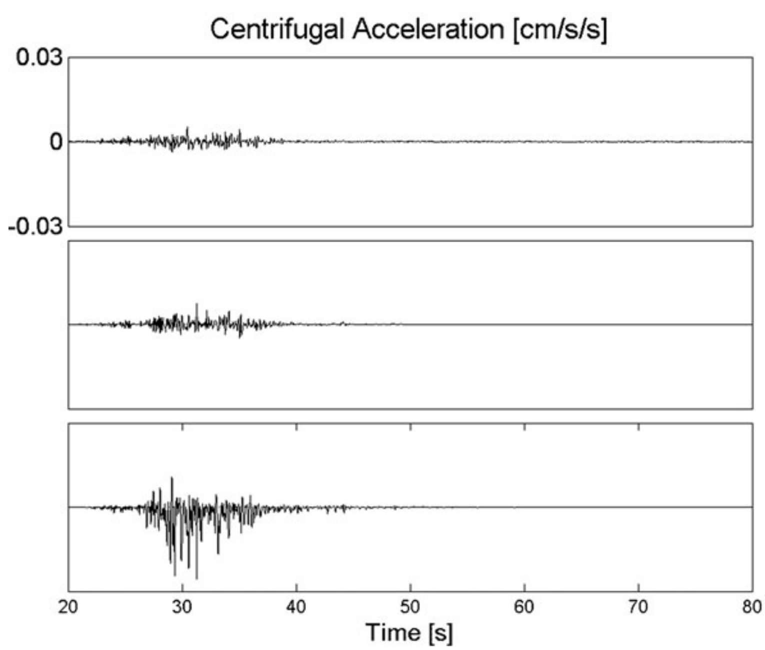

Fig. 5 Three-component centrifugal acceleration due to rotation motion

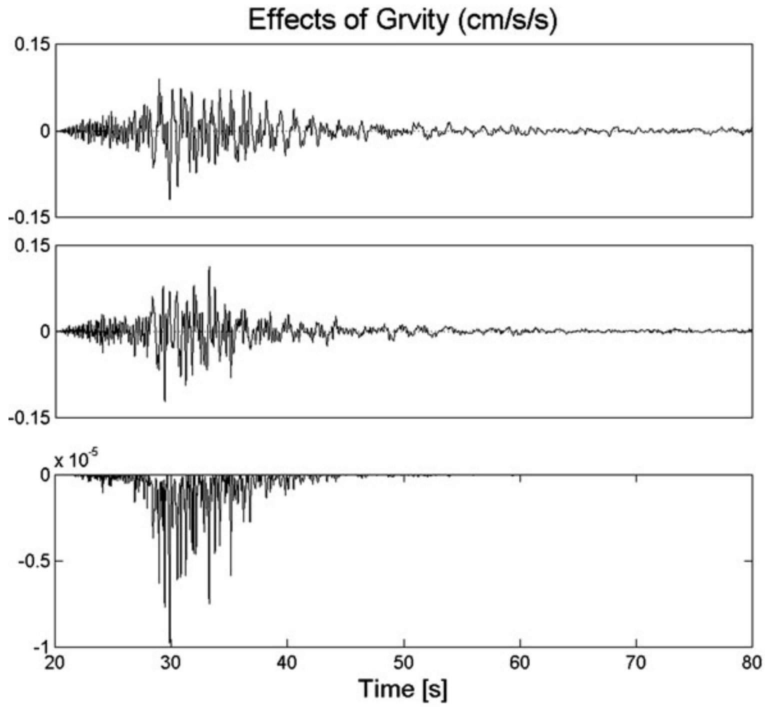

Fig. 6 Gravity effects on the three axis of the rotation frame

two horizontal components and to be negative. The negative value is expected because the tilt of the instrument always causes a reduction on the effect in the vertical direction. A smaller effect for the vertical component is also expected. For a small ground tilt, the horizontal component is proportional to the tilt angle while the vertical component will be proportional to the square of the tilt angle.

Solving the ordinary differential in Eq. (2) gives the three-component velocity waveforms in the rotation

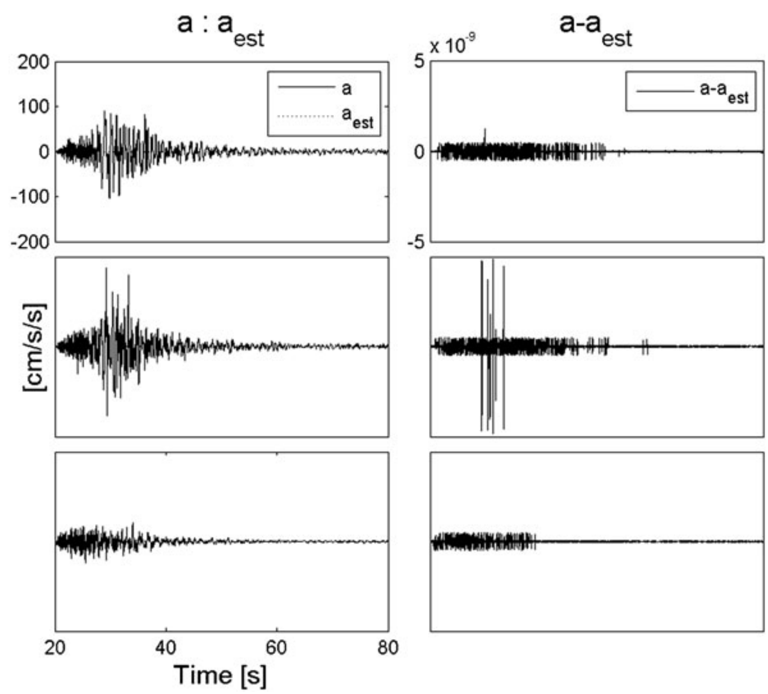

Fig. 7 Comparisons of acceleration waveform between "a" (by numerical differentiation of velocity waveforms) and "a_{est}" (by Eq. 2) are on the *left*. The differences between "a" and "a_{est}" are on the *right*

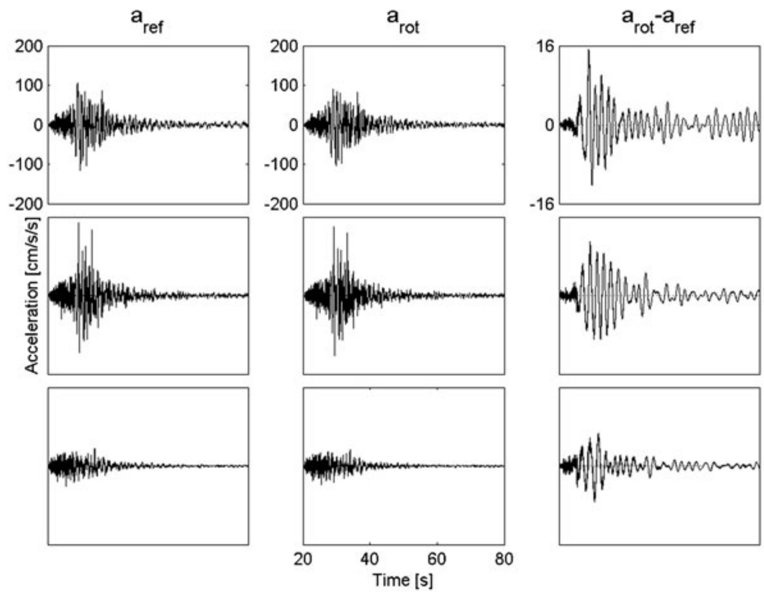

Fig. 8 The three-component accelerations on the reference frame are in the first column and the corresponding components on the rotational frame are in the second column. The differences between these two types of accelerations are shown in the third column

frame. There are two approaches that can be applied to calculate the acceleration waveforms in the rotation frame; the first substitutes the velocity back to Eq. (1) to obtain a_{est}, and, the other approach is using numerical differentiation of the velocity to give "a". Comparing results of these two approaches provides a check on the overall error in numerically solving the ordinary differential Eq. (4) and the numerical differentiation. Comparisons of overlapped waveforms plots are shown on the left side in Fig. 7 and the difference in these two waveforms is shown on the right side in Fig. 7. As shown in the figure, the difference is about 10^{-9} cm/s/s which is much smaller than the peak acceleration of 186 cm/s/s.

The maximum centrifugal acceleration, effect from gravity, and effect of the rotation frame are both small (0.03 cm/s/s and 0.14 cm/s/s). This result might have been expected because our data are not near-field and wave motions are expected to be nearly plane waves.

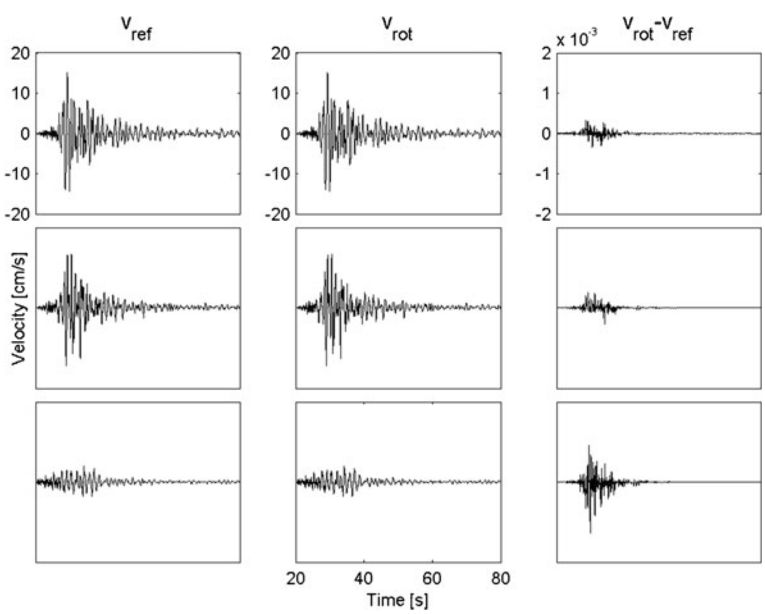

Fig. 9 The three-component velocities on the reference frame are in the first column and the corresponding components on the rotational frame are in the second column. The differences between these two types of accelerations are shown in the third column

The effects due to the rotation frame can be examined by comparing the waveforms in both frames. The acceleration waveforms in the reference and the rotation frame are shown in the first and second columns in Fig. 8 and their difference is given in the third column. The maximum difference is about 16 cm/s/s (about 10 %). This difference has lower frequency content than that of the original signal and is much larger than the combination of the centrifugal acceleration and gravity effects. It seems that this large difference in waveforms is related to the phase difference between two waveforms, but we are still unable to identify the cause of this large difference which warrants further investigation. The velocity waveforms in the reference and the rotational frame are shown in the first and second columns in Fig. 9 and their differences are given in the third column. The difference is about 0.0012 cm/s (about 0.01 %).

Due to limitations in the dataset, this study only estimates the effects of rotational motions in a limited frequency band from 0.1 to 20 Hz. Since the major signals for both rotational and translational data are below 15 Hz, the instrument corrections for the high frequency part are not that important for both data. The flat instrument response of the VSE-355 G3 can go down to 0.02 Hz, but the R1 data might have waveform distortions and phase drift below 1 Hz. Therefore, we need an instrument correction for R1 data. However, after considering the low-frequency noise, we select the lower-bound of the band–pass filter to be 0.1 Hz.

Common timing for the rotation rate and ground motion data is important in our analysis. This is the reason for selecting the strong-motion velocity waveform rather than the HWA019 acceleration data.

5 Conclusions

This study develops a numerical algorithm for estimating the effects of rotational motion on the strong-motion data using a set of six-component ground motions. Due to the limitation of rotation data, the estimation in this study is limited in a frequency band from 0.1 to 20 Hz. However, the algorithm itself does not have such limitation.

Effects of rotation motions on translational motions include centrifugal acceleration, gravity effects, and the effects of the rotation frame. Results show that all these effects have the same order of contribution to the strong-motion data. Since all these analyses are in time domain, our results provide some detailed features of these effects.

The centrifugal acceleration calculated in this study is 0.03 cm/s/s which is much larger than 0.000135 cm/s/s calculated base on Graizier's estimation (Graizer 2009). This discrepancy implies that the center of the rotation motion might be not at the fixed point of the pendulum. What cause this discrepancy warrants further studies.

The maximum difference between the corrected and uncorrected acceleration waveforms is about 16 cm/s/s (about 10 %). This difference has higher low-frequency content than that of the original signal and is much larger than the combination of the centrifugal acceleration and gravity effects. The cause of this large difference is not known and it needs further investigation.

Acknowledgments We are grateful to Dr. Zembaty and two anonymous reviewers for their valuable suggestions. This research was supported by Academia Sinica and the National Science Council, Taiwan, Republic of China. The HWA019 strong-motion data was provided by Central Weather Bureau, Taiwan. The support from these organizations is gratefully acknowledged.

References

Boore DM (2001) Effect of baseline corrections on displacements and response spectra for several recordings of the 1999 Chi-Chi, Taiwan, earthquake. Bull Seismol Soc Am 91(5):1199–1211

Boroschek RL, Legrand D (2006) Tilt motion effects on the double-time integration of linear accelerometers: an experimental approach. Bull Seismol Soc Am 96(6):2072–2089

Chiu HC (1997) Stable baseline correction of digital strong-motion data. Bull Seismol Soc Am 87(4):932–944

Clinton JF, Heaton TH (2003) Performance of the VSE-355G2 strong-motion velocity seismometer. Report to the IRIS-GSN subcommittee, Version II, California Institute of Technology, Pasadena, p 60

Graizer V (2005) Effect of tilt on strong motion data processing. Soil Dyn Earthq Eng 25(3):197–204

Graizer V (2009) Tutorial on measuring rotations using multi-pendulum systems. Bull Seismol Soc Am 99(2B):1064–1072

Graizer V, Kalkan E (2008) Response of pendulums to complex input ground motion. Soil Dyn Earthq Engin 28(8):621–631

Hutt CR, Evans JR, Yokoi I (2008) A brief test of the Tokyo Sokushin VSE–355G3 strong motion velocity seismometer. U.S. Geological Survey Open-File report 2008–1311, p 43

Lee WHK, Huang BS, Langston CA, Lin CJ, Liu CC, Shin TC, Teng TL, Wu CF (2009) Review: progress in rotation ground-motion observations from explosions and local earthquakes in Taiwan. Bull Seismol Soc Am 99(2B):958–967

Lin CJ, Huang HP, Liu CC, Chiu HC (2010) Application of rotation sensors to correcting rotation-induced effects on accelerometers. Bull Seismol Soc Am 100(2):585–597

Nigbor RL, Evans JR, Hutt CR (2009) Laboratory and field testing of commercial rotational seismometers. Bull Seismol Soc Am 99(2B):1215–1227

Pillet R, Virieux J (2007) The effects of seismic rotations on inertial sensors. Geophys J Int 171(3):1314–1323

Takeo M (2009) Rotation motions observed during an earthquake swarm in April 1998 offshore Ito, Japan. Bull Seismol Soc Am 99(2B):1457–1467